Journal of Solid State Chemistry 312 (2022) 123228

Contents lists available at ScienceDirect

Journal of Solid State Chemistry

journal homepage: www.elsevier.com/locate/jssc

Oxygen surface exchange properties and electrochemical activity of lanthanum nickelates

Artur J. Majewski [a,*], Anna Khodimchuk [b], Dmitriy Zakharov [b], Natalia Porotnikova [b], Maxim Ananyev [c], Ian D. Johnson [d], Jawwad A. Darr [d], Peter R. Slater [e], Robert Steinberger-Wilckens [a]

[a] School of Chemical Engineering, University of Birmingham, Birmingham, B15 2TT, UK
[b] Institute of High Temperature Electrochemistry, UB RAS, Yekaterinburg, ul. Akademicheskaya 20, Russia
[c] Federal State Research and Design Institute of Rare Metal Industry, ul. Electrodnaya 2, Moscow, 111524, Russia
[d] Department of Chemistry, University College London, London, WC1H 0AJ, UK
[e] School of Chemistry, University of Birmingham, Birmingham, B15 2TT, UK

ARTICLE INFO

Keywords:
Solid oxide cell
Oxygen electrode
La2NiO4+δ
La3Ni2O7-δ
La4Ni3O10-δ
Oxygen surface exchange
Isotope exchange

ABSTRACT

Oxygen surface exchange properties of lanthanum nickelates $La_2NiO_{4+\delta}$, $La_3Ni_2O_{7-\delta}$ and $La_4Ni_3O_{10-\delta}$ (LNOs) have been investigated using the Pulsed Isotope $^{18}O/^{16}O$ Exchange (PIE) technique in the temperature range 300–700 °C. The evaluation of the oxygen exchange rate from these lanthanum nickelates was conducted by measurement of isotope fractions $^{18}O_2$, $^{16}O^{18}O$, and $^{16}O_2$ in the effluent pulse at the exhaust from the reactor with a packed bed. The rates of oxygen heterogenous surface exchange (r_H), dissociative adsorption (r_a) and incorporation (r_i) were calculated. The oxygen surface exchange was found to vary between the three nickelates, with r_H decreasing between samples $La_3Ni_2O_{7-\delta} > La_4Ni_3O_{10-\delta} > La_2NiO_{4+\delta}$, which was attributed to a decreasing presence of Ni cations on the particle surfaces. Despite possessing the lowest oxygen surface exchange, $La_2NiO_{4+\delta}$ had the best electrode electrochemical performance, which was attributed to highly mobile interstitial oxygen atoms leading to the largest r_i (surface oxygen incorporation rate into the bulk) of the nickelates. This study reveals the key limiting factors determining lanthanum nickelate cathode performance in SOFCs, and we suggest avenues to improve these materials towards functional cathodes in devices.

1. Introduction

The considerable increase in renewable energy integration in electricity grids is leading to growing demand for energy storage systems. One option is the conversion of power to gas (P2G) and the employment of reversible fuel cells, acting as fuel cell or electrolyser, depending on grid needs. This has opened up renewed possibilities for a wider application of Solid Oxide Cells (SOC) as Fuel Cells (SOFCs) for efficient energy generation and Electrolysers (SOEs) for hydrogen and syngas production. Both SOC modes increasingly rely on oxygen electrodes composed of mixed conductors (both oxide ion and electronic charge carriers) for lower temperature operation. The performance of SOC decreases at lower temperature caused by ohmic losses in the electrolyte and the overpotential generated at the oxygen electrode. The oxygen electrode degradation issue is considered the biggest challenge for SOC in both electrolysis and fuel cell mode. Therefore, research on alternative, stable Mixed Oxygen Ionic and Electronic Conducting (MIEC) electrodes that may provide higher current density, is a priority research in the SOC field.

Lanthanum Nickelates (LNOs), as mixed ionic (O^{2-}) and electronic conducting oxides, are promising materials for SOC oxygen electrodes owing to their high electronic and ionic conductivity and high catalytic activity for oxygen reduction (for SOFC) and evolution (for SOE) oxygen electrode reactions and moderate thermal expansion coefficients (TEC) [1–4]. TEC values for LNOs were reported to be comparable with the common electrolytes, with the following values: $La_2NiO_{4+\delta}$ 13.8×10^{-6} K^{-1}, $La_3Ni_2O_{7-\delta}$ 13.2×10^{-6} K^{-1}, and $La_4Ni_3O_{10-\delta}$ 12.6×10^{-6} K^{-1} over the temperature range of 40–800 °C [3,5]. The advantage of an LNO based electrode is the absence of alkaline-earth cations that are reported to segregate from the Perovskite structure, resulting in electrode degradation [6]. As MIECs, Lanthanum nickelates offer the potential for lower operational temperatures, thus improving materials durability.

* Corresponding author.
E-mail address: a.j.majewski@bham.ac.uk (A.J. Majewski).

https://doi.org/10.1016/j.jssc.2022.123228
Received 13 February 2022; Received in revised form 27 April 2022; Accepted 6 May 2022
Available online 15 May 2022

Lanthanum nickelates $La_{n+1}Ni_nO_{3n+1}$ have Ruddlesden-Popper (R–P) structures $(ABO_3)_nAO$, which consist of intergrowths of *n* Perovskite-type layers $(LaNiO_3)_n$ with rock-salt-type layers (LaO) along the crystallographic *c* direction [2,7,8]. The electronic conductivity is several orders of magnitude higher than the ionic conductivity for these LNO compounds ($\sigma_{el} \gg \sigma_{ion}$). This LNO family of compounds, including $La_2NiO_{4+\delta}$, $La_3Ni_2O_{7-\delta}$ and $La_4Ni_3O_{10-\delta}$, have been suggested as promising candidates for SOC electrodes and oxygen permeation mixed ionic-electronic conducting membranes [9,10].

The most extensively studied material, $La_2NiO_{4+\delta}$, was reported to have higher oxygen diffusivity and surface oxygen exchange than that of the state of the art $La_xSr_{1-x}Co_yFe_{1-y}O_{3-\delta}$ (LSCF) [11,12] and $La_xSr_{1-x}MnO_{3\pm\delta}$ (LSM) oxygen electrodes [13] due to a lower activation energy for ionic conductivity.

$La_2NiO_{4+\delta}$ is an interesting system as it accommodates oxygen excess in interstitial sites in the LaO rock-salt layers [14], which allows rapid oxygen transport through the ceramic material. The incorporated interstitial oxide ions can be compensated by Ni^{3+} or a combination of an oxidized lattice oxygen ion O^- and Ni^{3+} cation defects [14,15]. The oxygen transport via vacancies in the $La_2NiO_{4+\delta}$ Perovskite layer is low. However, the literature data for the oxygen surface exchange coefficient (*k*) and oxygen tracer diffusion coefficient (*D*) for $La_2NiO_{4+\delta}$, show a large distribution of values due to different materials synthesis procedures, microstructure, etc. [1,16]. Despite these inconsistencies, the rate-determining step for $La_2NiO_{4+\delta}$ has been found to be the dissociative adsorption of oxygen [16,17], with the activation energy for the surface exchange found to be approximately double that of the diffusion process [11].

Despite these reported advantages, significant degradation was observed for $La_2NiO_{4+\delta}$ during SOFC or SOE operation. The applicability of $La_2NiO_{4+\delta}$ as SOC Intermediate Temperature (IT) oxygen electrode is also limited by chemical reactions with YSZ above 900 °C and with CGO above 700 °C [18]. Lee and Kim [19] also observed that high calcination and sintering temperature affected mass transfer resistance of $La_2NiO_{4+\delta}$ electrodes. In addition, the electronic conductivity of $La_2NiO_{4+\delta}$ was reported to be low [20]. To improve the stability, a nano-scale structure produced by infiltration into an electrolyte material scaffold was proposed [21]. Doping with alkaline earth metal cations was also reported to improve the electronic conductivity [22] but reduced the oxygen transport properties and surface reactivity [23], reducing the electrochemical performance. Also, the level of interstitial oxygen for $La_2NiO_{4+\delta}$, decreases when doping with alkaline-earth metals [23].

The electrical conductivity of $La_{n+1}Ni_nO_{3n+1}$ was reported to increase with the number of Perovskite layers in a formula unit (*n*) resulting in values of 63, 100 and 250 S cm^{-1} at 600 °C in ambient air, for n = 1, 2 to 3, respectively [1–4,12,24]. Song et al. [25] reported slightly higher electrical conductivity value probably related to higher sample density. Metallic behaviour was also reported for the $La_4Ni_3O_{10-\delta}$ phase due to the high Ni content [3,4]. The electronic conductivity of R-Ps phases increases with the *n* parameter due to the increase in the number of Perovskite layers responsible for this electronic conduction. In addition, the relative stabilities for $La_3Ni_2O_{7-\delta}$ and $La_4Ni_3O_{10-\delta}$ were found to be higher than for $La_2NiO_{4+\delta}$ due to increased Ni^{3+} content that is more stable in air at IT [3,24,26]. Increasing the number of Perovskite layers, improves the resistance to Cr poisoning [27]. Good LNO ionic and electronic conductivity can be achieved by a formulation of graded electrodes composed of a mixture of $La_2NiO_{4+\delta}$ with higher-order nickelates $La_3Ni_2O_{7-\delta}$ or $La_4Ni_3O_{10-\delta}$ [1]. Other applications of LNOs include coating metallic interconnects [28] or the oxidation of hydrocarbons (chemical looping) [29].

To better understand the processes at the oxygen electrode, there is a need to analyse the interaction between the electrode and the gaseous phase. In the literature, oxygen kinetics are usually described by the oxygen surface exchange coefficient *k*, the oxygen heterogenous exchange rate r_H, or the oxygen diffusion coefficient *D*. The performance of oxygen electrodes depends on the oxygen surface exchange because it affects the overall kinetics of porous electrodes [11]. Therefore, the gas/solid interfaces of oxygen electrodes play an important role in the development of such electrodes. Several reports are found in the literature on $La_2NiO_{4+\delta}$ oxygen surface exchange properties. However, for $La_3Ni_2O_{7-\delta}$ and $La_4Ni_3O_{10-\delta}$, this information needs affirmation. To the authors' knowledge the only report on $La_3Ni_2O_{7-\delta}$ and $La_4Ni_3O_{10-\delta}$ oxygen transport properties [25] showed that the oxygen self-diffusion coefficients (Ds) decreased with the order of parameter *n*. Therefore, the goal of this study is to determine the oxygen surface exchange properties for $La_3Ni_2O_{7-\delta}$, $La_4Ni_3O_{10-\delta}$, and compare with properties of $La_2NiO_{4+\delta}$, using the pulse ^{18}O-isotope exchange method. Knowledge of the rate of the oxygen surface exchange will help to understand activity in catalytic reactions.

Furthermore, literature reports on the area specific resistance of LNOs are contradictory. Some authors reported that an increase in the number of Perovskite layers, decreased the overall resistance of the LNO cells. For example, for symmetrical cells with a $La_{0.9}Sr_{0.1}Ga_{0.8}Mg_{0.2}O_{3-\delta}$ (LSGM) electrolyte, Amow et al. [3] reported lower Area Specific Resistance (ASR) with increasing *n* and attributed this to the increase in electrical conductivity. A similar effect was reported by Choi et al. [2], however, they tested LNOs electrodes as a composite with YSZ and the formation of a long triple-phase boundary (TPB) could account for the performance of the cells. The opposite effect, similar to what is presented in this work, was reported by Sharma et al. [1,24] for cells with a $Ce_{0.9}Gd_{0.1}O_{2-\delta}$ (CGO) electrolyte and by Woolley et al. [30] with an LSGM electrolyte. Therefore, more research is needed to explain how the microstructure, presence of impurity at the interface, and the electrolyte properties affect the ASR of the LNO cells.

Herein, the authors report the effect of LNO composition and phase on the oxygen surface exchange kinetics and electrochemical performance, revealing that $La_2NiO_{4+\delta}$ possessed the lowest polarisation resistance and the best electrode performance. The dependence of the oxygen heterogenous exchange rate was analysed with the rates of oxygen dissociative adsorption and incorporation rate on the temperature in the context of surface composition and defect structure. This suggests future research directions that could lead to further improvements in LNOs towards functional SOFC cathode materials.

2. Experimental

2.1. Materials preparation

$La_2NiO_{4+\delta}$ electrode material was synthesized by the standard co-precipitation method, with preliminary synthesis at 950°C for 2 h and final annealing at 1,250 °C. The product was then ground and sieved to a size of 20 μm.

The $La_3Ni_2O_{7-\delta}$ and $La_4Ni_3O_{10-\delta}$ samples were synthesized using an initial continuous hydrothermal flow synthesis method to precipitate an intimate mixture of the respective homometallic oxides, that were then heat treated to give phase pure materials. The synthesis pathway has been described elsewhere, with final heat treatment at 1,100 °C for 5 h in ambient air [31].

All tested powders were well crystallised. The sintering temperature was determined by the structural stability of lanthanum nickelates as reported in the literature [30,32]. For the $La_3Ni_2O_{7-\delta}$ and $La_4Ni_3O_{10-\delta}$, it was impossible to fabricate dense pure phase pellets. According to the literature [30] and also from preliminary results, the stability of those materials was affected by exposure to a temperature above 1,200 °C (due to the resultant oxygen loss) and decomposition into the $n = 1$ $La_2NiO_{4+\delta}$ occurred. Pellets sintered below 1,200 °C were not dense enough for the oxygen isotope exchange with the gas phase equilibration experiment. For those samples, complex sintering at high oxygen partial pressure or post-sintering oxidation is required for the formation of dense pellets [33]. Song et al. [25] reported fabrication of $La_3Ni_2O_{7-\delta}$ and $La_4Ni_3O_{10-\delta}$ relatively dense pellets sintered at 1,300 °C. However, even using the complex procedure with 2 days milling and over 200 h of post-sintering

results in pellets with impurity up to 4%. Nevertheless, the properties of the interaction of oxygen with the surface can be quantitatively measured from powder samples using oxygen pulsed isotopic exchange.

The $Ce_{0.8}Sm_{0.2}O_{1.9}$ electrolyte powder was prepared using a glycerol-nitrate route. The obtained powder was annealed at 1,300 °C for 4 h, ground and dry-pressed at 6 MPa into tablets with the subsequent sintering in ambient air at a temperature of 1,650°C for 5 h $Ce_{0.8}Sm_{0.2}O_{1.9}$ has a fluorite structure (space group Fm-3m, a = 5.4347(1) Å).

2.2. Materials characterisation

The phase purity and crystal structure of the samples were determined by powder X-Ray Diffraction (XRD). XRD patterns were collected with a D8 ADVANCE (Bruker) diffractometer with Cu-Kα radiation at room temperature in ambient air. The structural refinements (the lattice parameters and phase fractions) were performed with GSAS-II software based on the Rietveld method [34].

Nonstoichiometric oxygen coefficient (δ) of the tested materials was measured by thermogravimetric analysis (TGA) in a reducing atmosphere (5%H_2:N_2, 50 ml min^{-1}), which used the mass loss observed to deduce the original oxygen content. The δ value was calculated assuming that the final product of the reduction process for all tested $La_{n+1}Ni_nO_{3n+1}$ samples was La_2O_3 and Ni^0, with the excess oxygen removed in the form of water. TGA profiles were analysed using a Netzsch 209F1 instrument, evaluated between room temperature and 1,000 °C, at a heating rate of 5 °C·min^{-1}, with a sample mass in the range 10–20 mg.

Analysis of the microstructure and chemical elemental composition of sintered powders were conducted using an SEM Hitachi TM3030Plus equipped with Quantax70 EDX. The deviation of the cationic composition from the theoretical value was below 2%.

The surface area analysis of the powders was performed via the Brunauer-Emmett-Teller (BET) method on a Sorbi N.4.1. Samples were preliminarily degassed for 1 h under a He flux at 200 °C. The BET surface area was determined as 0.7, 1.2 and 1.3 m^2g^{-1} for $La_2NiO_{4+\delta}$, $La_3Ni_2O_{7-\delta}$ and $La_4Ni_3O_{10-\delta}$, respectively. These values were used for the oxygen exchange rate calculations.

For Low-Energy Ion Scattering (LEIS) tests, the obtained powders were ground, sieved to 100 μm, and pressed into 6 mm diameter pellets with a weight of 0.5 g. The pellets were sintered at 1,100 °C for 4 h in ambient air. The LEIS study was carried out using a Thermo NEXSA spectrometer with monochromated Al kα as dual-beam low-energy electron/ion source for the X-ray source. The analysis spot size was 200 × 100 μm, at 300 K with Ar clean with ion beam settings: 4,000 eV, Ar+, 30 s, 0.4 mm raster. Depth of measurement values was based on sputter rates determined through the analysis of a tantalum oxide calibration standard.

2.3. Oxygen isotopic exchange experiment

The idea of the Pulsed Isotope Exchange (PIE) technique was suggested by Bouwmeester for the first time in reference [35]. PIE in a flow reactor with gas-phase analysis, was applied to characterise the oxygen surface exchange activity of the LNO samples. The PIE measurements were used to calculate the oxygen heterogenous surface exchange (r_H) rate and the rates of the three exchange types, according to the Boreskov and Muzykantov theory [36]. Before the pulsing of labelled ^{18}O through the reactor, the sample was flushed with the carrier gas 21% $^{16}O_2$:He at 900 °C for 30 min to remove any impurities (adsorbates). PIE was carried out using 21%$^{18}O_2$/N_2 pulses in the temperature range of 350–700 °C. The oxygen purity was 99.9996%, the labelled oxygen was enriched by the ^{18}O isotope to 83%. The surface oxygen exchange parameters were calculated by analysis of $^{18}O_2$ and $^{16}O^{18}O$ molecule fractions in the gas phase at the reactor exit over time, using isotope kinetic equations as described elsewhere [10,16,35,37–39]. During the experiments, the response from the surface and bulk of the tested oxide powders resulted in changes to the gas-phase composition. Powder samples in the mass range 300–350 mg were supported by quartz wool plugs in a quartz continuous-flow packed-bed microreactor with an inner diameter of 2 mm and a bed length of ca. 10 mm. When the chemical equilibrium for the gas-carrier was achieved at the required temperature, the pulse of a mixture of $^{18}O_2$:N_2 was injected using a loop with 1,000 μl pulse. The oxygen partial pressure in the pulse was the same as in the carrier gas to maintain chemical equilibrium. The response to the ^{18}O-enriched pulse feed through the reactor was monitored by mass spectrometric analysis of the gaseous phase fractions. The gas mass spectrometer allowed analysis in the distribution of isotopologues $^{18}O_2$, $^{16}O^{18}O$ and $^{16}O_2$ in the effluent pulse at the exit of the reactor. The used packed bed length was as described in reference [10] to assure the governance of oxygen exchange by the surface reaction, and not by bulk oxygen diffusion. Pulse injection results were analysed at various temperatures in reference to experiments carried out at low temperatures when the sample had no activity to oxygen isotopic exchange. The temperature range for which the oxygen exchange rate was analysed was limited to a maximum of 700 °C because of the amount of ^{18}O isotope injected and the contribution of diffusion (sample porosity).

2.4. Electrochemical cell preparation and characterisation

2.4.1. Symmetrical cells

O_2, $La_{n+1}Ni_nO_{3n+1}$ | $Ce_{0.8}Sm_{0.2}O_{1.9}$ | $La_{n+1}Ni_nO_{3n+1}$, O_2

(n = 1, 2 and 3) were fabricated by a screen-printing method. The preparation technique was comprised of two steps: initial deposition by screen printing of the electrode slurry with organic binding, which prevented the trickling of the slurry onto the electrolyte. This slurry was subsequently sintered at 1,100 °C for 1 h in air. Both electrodes were prepared and sintered in one step. The area of the $La_{n+1}Ni_nO_{3n+1}$ (n = 1, 2 and 3) electrodes was 0.36 cm^2. After sintering, the electrodes had a porous structure (Fig. 6e and f).

Electrochemical measurements of the symmetric cells were carried out by Electrochemical Impedance Spectroscopy (EIS) using the VersaSTAT 4000 in the temperature range 600–800°C in air. The electrical contacts were provided by pressing between Pt-grids. Impedance spectra were registered in the frequency range of 0.05–10^5 Hz at the AC amplitude of 20 mV. The scheme of the experimental setup for electrochemical measurements was described elsewhere [40]. Both the electrochemical measurements and the oxygen isotope exchange were carried out under similar conditions to correlate results.

3. Results and discussion

3.1. Chemical composition of the bulk and the surface

Oxygen nonstoichiometry of tested samples was studied using the thermogravimetric technique. Fig. 1 shows the temperature dependencies of the sample mass in the temperature range of 30 to 1,000 °C.

In agreement with the literature the reducing atmosphere (5%H_2:N_2) treatment showed a two-stage mass reduction process, attributed to the loss of oxygen. At a low-temperature range up to 380 °C, the plots are nearly horizontal with no mass reduction. In the first stage (range 380–498 °C), reduction of mass by 0.5, 1.06 and 1.73% was observed for $La_2NiO_{4+\delta}$, $La_3Ni_2O_{7-\delta}$, $La_4Ni_3O_{10-\delta}$, respectively. The oxygen released at low temperature can be assigned to the reduction of Ni^{3+} to Ni^{2+} and the small amount of NiO impurity detected by XRD, whereas the weight loss at the high-temperature range, is most likely related to the reduction of LNOs to Ni^0 and La_2O_3. The two-step reduction process found for all compositions was in agreement with the literature reports [25,41]. The Temperature-Programmed Reduction (TPR) results suggested decreasing stability of the LNO samples with increasing n in the reductive

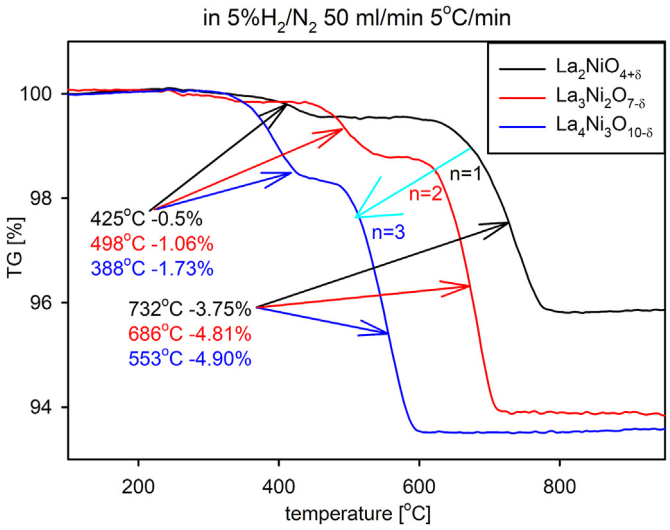

Fig. 1. TGA plot for $La_2NiO_{4+\delta}$, $La_3Ni_2O_{7-\delta}$, $La_4Ni_3O_{10-\delta}$; under 5%H_2:N_2 50 ml min^{-1}, heating rate 5 °C·min^{-1}.

atmosphere. There was no further oxygen loss at a temperature above 600, 700, and 800 °C for $La_4Ni_3O_{10-\delta}$, $La_3Ni_2O_{7-\delta}$, $La_2NiO_{4+\delta}$, respectively. The H_2-TPR measurements showed a lower reduction temperature for $La_4Ni_3O_{10-\delta}$. In general, the reduction temperature decreased with an increase in the n factor in $La_{n+1}Ni_nO_{3n+1}$. The calculated δ value was 0.25(5) as hyperstoichiometric oxygen with interstitial positions for $La_2NiO_{4+\delta}$, which is consistent with values reported in the literature for this class of compounds with δ from 0.16 to 0.25 [23,25,42]. For $La_3Ni_2O_{7-\delta}$ the δ value was 0.23(1), and for $La_4Ni_3O_{10-\delta}$ the δ value was 0.63(7) as oxygen deficiency. The obtained δ value for $La_3Ni_2O_{7-\delta}$ and $La_4Ni_3O_{10-\delta}$ was in the same order but slightly larger than reported by Song et al. [25] with oxygen deficiency δ 0.08 for $La_3Ni_2O_{7-\delta}$ and 0.15 for $La_4Ni_3O_{10-\delta}$. However, sample thermal history is known to influence oxygen stoichiometry. Aside from the differences observed with increasing n value, the oxygen nonstoichiometry aspect can depend on the synthesis method [43], with over-stoichiometric oxygen $\delta = -0.05$ reported for $La_3Ni_2O_{7-\delta}$ (in contrast to the sub-stoichiometry observed in this report) [1]. Moreover, a slight deviation in the La:Ni metal stoichiometries can result in a large deviation in the oxygen stoichiometry [31], and under SOC operating conditions the nonstoichiometric oxygen content of LNO depends also on oxygen partial pressure and temperatures [44]. Regardless of this variability, the presence of oxygen nonstoichiometry in LNO compounds results in comparatively good O^{2-} ionic conductivity, and opens the potential for these materials to work as SOC oxygen electrodes. However, the oxygen transport mechanism for $La_2NiO_{4+\delta}$ is different than for $La_3Ni_2O_{7-\delta}$ and $La_4Ni_3O_{10-\delta}$.

The microstructure of the electrode powders of the sintered LNO electrode materials is presented in SEM scans, Fig. 2a–c, where all samples showed high porosity. The mean particle size for $La_2NiO_{4+\delta}$ was around 2 μm, for $La_3Ni_2O_{7-\delta}$ around 1–2 μm, while for $La_4Ni_3O_{10-\delta}$ it was around 1 μm, according to SEM data. The particle size was in good agreement with porosity and surface area measured by BET of 0.69, 1.23 and 1.31 m^2 g^{-1}, respectively. Similar results for the relationship between the LNO's n parameter and the porosity and particle size were reported by Choi et al. [2].

The phase composition of the LNO powder samples was analysed at room temperature by XRD (Fig. 2d). The refinement results confirmed that sintered $La_2NiO_{4+\delta}$, $La_3Ni_2O_{7-\delta}$, $La_4Ni_3O_{10-\delta}$ powders were almost single phase with the expected Ruddlesden-Popper structures. No evidence the $La_6Ni_5O_{16}$ impurity phase, as previously reported, was observed [45]. A few weak peaks related to NiO and lanthanum oxide phase impurities were observed in the XRD patterns, however, their refined content was too small to influence the oxygen isotope kinetic study results. The lattice parameters calculated by the Rietveld method (Table 1) were in good agreement with previously reported data [1,25].

Fig. 3 presents the LEIS spectra of the outermost atomic layers of the polycrystal samples (a) $La_2NiO_{4+\delta}$, (b) $La_3Ni_2O_{7-\delta}$, and (c) $La_4Ni_3O_{10-\delta}$. Only oxygen, nickel and lanthanum were detected. Obtained peaks were relatively broad because measurements were made on compacted powder samples.

The LEIS analysis showed that the surface characteristics for

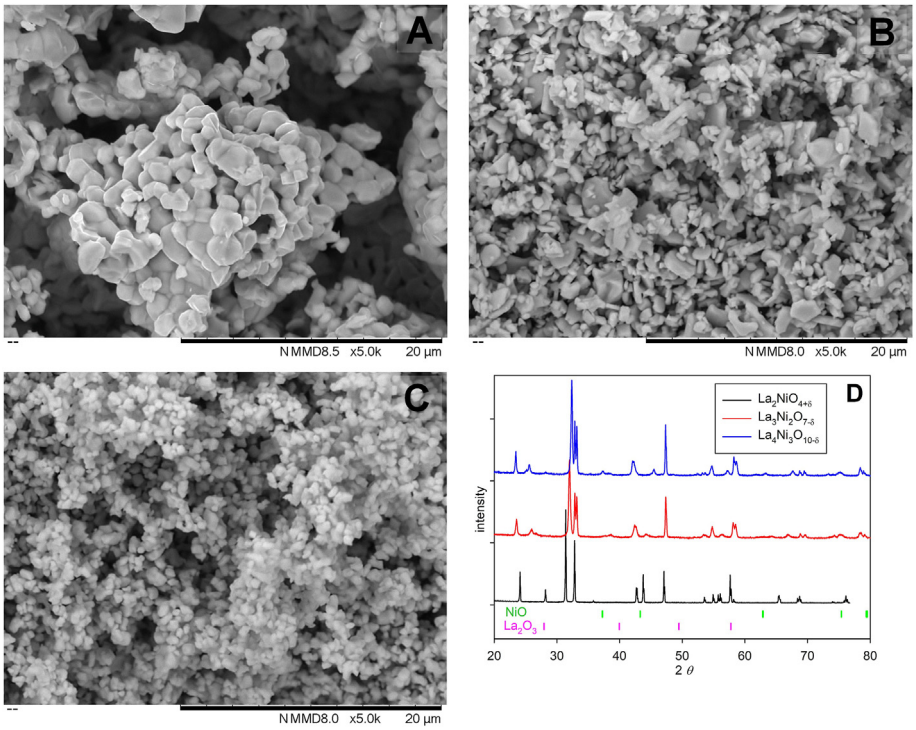

Fig. 2. SEM images of (a) $La_2NiO_{4+\delta}$, (b) $La_3Ni_2O_{7-\delta}$, (c) $La_4Ni_3O_{10-\delta}$ powders; (d) X-ray powder diffraction pattern of $La_2NiO_{4+\delta}$, $La_3Ni_2O_{7-\delta}$ and $La_4Ni_3O_{10-\delta}$.

Table 1
LNO lattice parameters obtained from the XRD refinement by GSAS (details of Rietveld refinement are provided in supplementary materials).

Crystal system	Unit cell [Å]			Vol [Å^3]	Theoretical density[a] [g·cm^{-3}]
	a	b	c		
$La_2NiO_{4+\delta}$	5.4612(6)	5.4612(6)	12.6798(8)	378.18(2)	7.062
$La_3Ni_2O_{7-\delta}$	5.4048(6)	5.4520(1)	20.4713(8)	603.23(8)	7.114
$La_4Ni_3O_{10-\delta}$	5.4120(7)	5.4609(8)	27.9899(6)	827.24(9)	7.160

[a] oxygen nonstoichiometry was not included.

$La_2NiO_{4+\delta}$ differed from those for $La_3Ni_2O_{7-\delta}$ and $La_4Ni_3O_{10-\delta}$. For all LNOs, the Ni coverage decreased at the outer surface. However, the measurements revealed that Ni was not present in the outermost atomic layer (0 nm) only for $La_2NiO_{4+\delta}$. This confirmed the previously reported results for both single crystal [46–50] and polycrystalline materials [16], of predominant A-site cation coverage at the outermost surface for $La_2NiO_{4+\delta}$. The results revealed the absence of surface Ni, which is a property of the oxide independent of microstructure. It is important to take this into consideration when one considers the surface exchange kinetics of the porous electrode, which displays microstructure as an average between polycrystalline and powdered since it has boundaries between the grains and high specific surface area. Therefore, we can assume there was also no Ni in the outermost layer of the $La_2NiO_{4+\delta}$ oxide porous electrode. Wu et al. [46] reported that the absence of Ni is caused by the decomposition of $La_2NiO_{4+\delta}$, and the formation of thermodynamically favourable higher-order R–P phases and La_2O_3. However, from the presented results (Fig. 3b and c) for $La_3Ni_2O_{7-\delta}$ and $La_4Ni_3O_{10-\delta}$ the absence of Ni in the outermost atomic layer was not detected. Therefore, it can be assumed that the La_2O_3 formation is responsible for the absence of Ni on the surface of $La_2NiO_{4+\delta}$.

In addition, LEIS analysis detected impurities in the first monoatomic layer of $La_2NiO_{4+\delta}$, which was probably Si as reported in references [16, 51]. However, EDX did not confirm the presence of Si. Apparently, the impurities' concentration was low and below the EDX detection level. The origin of this Si impurity remained unclear. It was probably related to the fabrication technique (the sample was synthesized by the co-precipitation method) or resulted from precursor material contamination, since the LEIS tests were conducted using freshly sintered samples. The impurity was not detected for $La_3Ni_2O_{7-\delta}$ or $La_4Ni_3O_{10-\delta}$ that were synthesized using a continuous hydrothermal flow synthesis. Furthermore, the intensity of the oxygen peak in the outermost atomic layer 0 nm (Fig. 3d) was higher for $La_2NiO_{4+\delta}$ than for $La_3Ni_2O_{7-\delta}$ or $La_4Ni_3O_{10-\delta}$. Therefore, the structure and chemistry properties for the bulk differed from those for the surface for $La_2NiO_{4+\delta}$, which was not the case for $La_3Ni_2O_{7-\delta}$ and $La_4Ni_3O_{10-\delta}$. It should be noted that for the higher *n* index in RPs, higher was the overall Ni/La ratio. The demonstrated absence of nickel in the outermost atomic layer for $La_2NiO_{4+\delta}$ suggested lanthanum and oxygen segregation, observed at room temperature. Extended annealing time or temperature was reported to lead to an increase in the concentration of one of the elements in the surface layer of Perovskites due to segregation [37,50]. Therefore, the segregation is likely to have occurred as part of the thermal history of the sample and

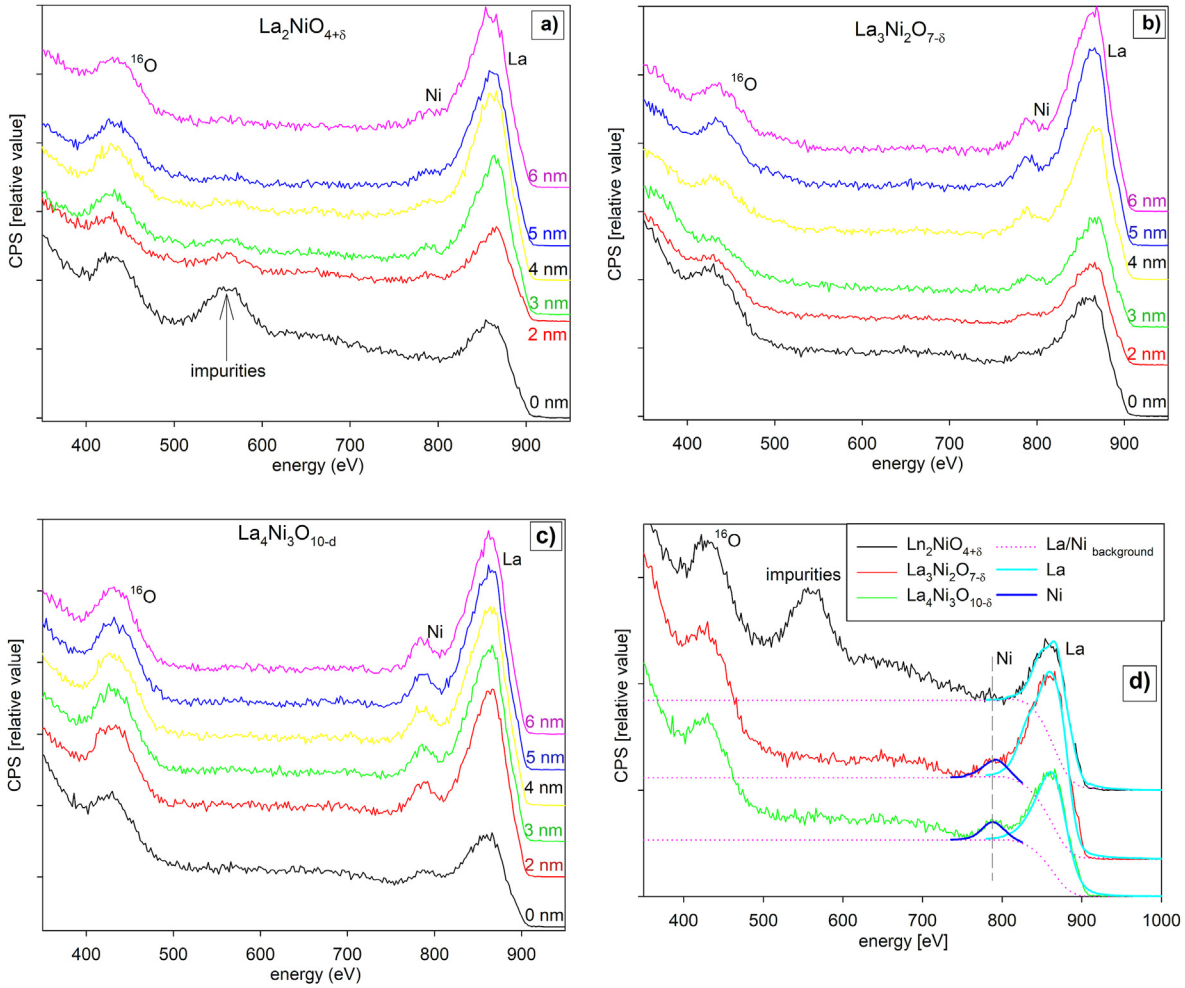

Fig. 3. LEIS scans for a) $La_2NiO_{4+\delta}$, b) $La_3Ni_2O_{7-\delta}$, c) $La_4Ni_3O_{10-\delta}$, and d) 0 nm layer for all samples.

associated with surface termination.

The plateau of bulk composition was observed for the outermost surface below the 4–5 nm region, as shown in the profiles (Fig. .3a–c). That was below the 2 nm region reported by Wu et al. [50] for single-crystal films. The difference can be related to the surface roughness of compressed polycrystalline powders. Overall, the different composition of the outer-most layer of $La_2NiO_{4+\delta}$ resulted in different interaction of oxygen from the gas phase with the structural oxide ions, as presented by the PIE results.

3.2. The pulse technique - surface reactivity

The pulse technique of $^{18}O_2$–$^{16}O_2$ isotopic exchange, allows analysis of surface oxygen exchange properties. Results provide information on kinetics and mechanism of the oxygen exchange reaction. Mechanistic information of the oxygen surface exchange reaction is obtained from the gaseous phase analysis. The details of the two-step model calculations and theory of dissociative adsorption and incorporation distribution based on the three types of exchange type rate models has been described elsewhere [16,35,52,53]. In general, the oxygen surface exchange under the pulse technique was calculated from the residence time and the uptake of ^{18}O by the sample according to the Boreskov and Muzykantov [36] theory. Oxygen surface exchange kinetics were analysed based on the two-step model, including two consecutive steps: dissociative adsorption of oxygen (1) and incorporation of oxygen adatoms into the crystal lattice (2). This two-step model includes two consecutive stages of oxygen dissociative adsorption and incorporation:

$$O^{18}O + O_a \leftrightarrow^{r_a} O^{16}O + O_a. \quad (1)$$

$$O_a + O_s \leftrightarrow^{r_i} O_a + O_s \quad (2)$$

where O_a is the oxygen adatom and O_S is the incorporated oxygen. The calculated oxygen heterogenous surface oxygen exchange rate (r_H) corresponds to the amount of oxygen from the gaseous phase that interacted with a specific area of the lattice per time.

The amount of a sample and the injected volume of ^{18}O atoms, were selected to have a commensurate amount of oxygen atoms in analysed samples and ^{18}O atoms in a pulse. The pulse isotopic exchange technique allowed measurements of oxygen equilibrium surface exchange rates and analyses of factors governing that exchange process. Since the PIE technique does not require high-temperature pre-sintering, this allows analysis of surface oxygen exchange for samples that would decompose at the sintering temperature. The surface exchange rate was calculated from ^{18}O atom residence time and the surface area of the tested oxides. The uptake of ^{18}O by the tested oxides was evaluated from the difference between the concentration of the ^{18}O tracer in the calibrated injected pulse and the effluent. Oxygen atoms from the ^{18}O-containing gaseous phase pulse passing through the reactor bed were adsorbed (r_a) and incorporated (r_i) into the oxide lattice, with ^{16}O released to the gas phase for every successful exchange event. Sometimes not all the amount of oxygen in the solid oxide is exchangeable [54]. However, in the PIE technique, the amount of injected $^{18}O_2$ sotope tracer is small compared to the amount of oxygen in the solid oxide.

Fig. 4a–d shows the tracer diffusion studies and temperature dependency of oxygen isotope species $^{18}O_2$ (X_{36}), $^{16}O^{18}O$ (X_{34}), $^{16}O_2$ (X_{32}) fractions and the total fraction of the ^{18}O isotope (α) in the gaseous phase after passing through the reactor bed.

The obtained experimental data for the oxygen isotope fractions at the exhaust from the reactor (from the corresponding pulse) as a function

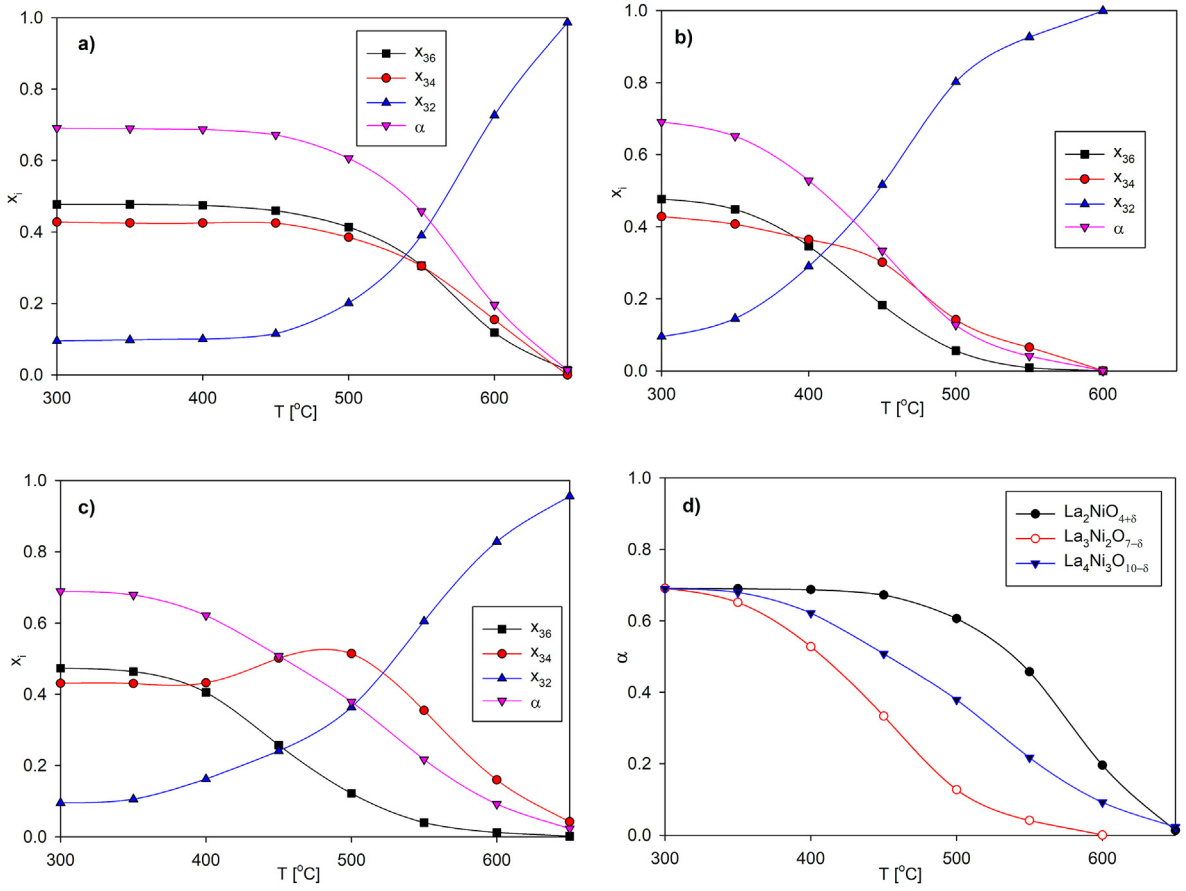

Fig. 4. Oxygen isotope fractions ($^{18}O_2$, $^{16}O^{18}O$ and $^{16}O_2$) as a function of temperature from pulse isotopic exchange measurements on a) $La_2NiO_{4+\delta}$, b) $La_3Ni_2O_{7-\delta}$, c) $La_4Ni_3O_{10-\delta}$, and d) α - molar fractions with oxygen ^{18}O, mass 34 and 32 ($\alpha = 1/2^{16}O^{18}O + {}^{18}O_2$), $pO_2 = 0.21$ atm.

of temperature for $La_2NiO_{4+\delta}$ (a), $La_3Ni_2O_{7-\delta}$ (b) and $La_4Ni_3O_{10-\delta}$ (c) are presented in Fig. 4. Isotope fractions were calculated from the integrated peak areas of mass spectroscopic data for $^{18}O_2$ and $^{16}O^{18}O$ obtained from PIE measurements, with $^{16}O_2$ calculated as balance.

$$X_{32} + X_{34} + X_{36} = 1 \quad (3)$$

The $^{18}O_2$ molar fraction from oxygen mass 34 ($^{16}O^{18}O$) and 32 ($^{16}O_2$) were calculated from the corresponding pulse integral values and the relationship:

$$\propto = X_{36} + 0.5X_{34} \quad (4)$$

The thermally activated oxygen exchange increased with temperature, resulting in the incorporation of 100% of the injected pulse of $^{18}O_2$ at a temperature above 700 °C for all tested samples under the tested conditions. The uptake of ^{18}O by the tested oxides, increased at elevated temperature. Correspondingly, the $^{18}O_2$ and the associated $^{16}O^{18}O$ isotope fraction at the reactor exhaust, decreased with increasing temperature. The behaviour for the three tested LNOs varied, caused by the nature of the oxides. The oxygen exchange rate varied with the temperature at constant feed/sweep gas flow and constant oxygen partial pressure. The observed decrease in $^{18}O_2$ fraction was balanced by an increase in $^{18}O^{16}O$ and $^{16}O_2$ fractions. For the $La_2NiO_{4+\delta}$ sample, the oxygen isotope surface exchange started at approx. 500 °C, similar to what was stated in previous reports [11] (Fig. 4a) while for $La_3Ni_2O_{7-\delta}$ and $La_4Ni_3O_{10-\delta}$ the oxygen isotope surface exchange started at a lower temperature around 350 °C (Fig. 4b and c), suggesting differences in the surface characteristics of these phases. The oxygen surface activity was in the order $La_3Ni_2O_{7-\delta} > La_4Ni_3O_{10-\delta} > La_2NiO_{4+\delta}$ under the equilibrium at the tested conditions. The obtained results thus showed higher surface activity of the slightly oxygen-deficient $La_3Ni_2O_{7-\delta}$ compared to $La_4Ni_3O_{10-\delta}$ and $La_2NiO_{4+\delta}$. The surface activity was therefore not in correlation with the lattice oxygen content (δ parameter) or Ni:O content.

To explain the mechanisms responsible for the absence of such correlation, an analysis of the rate for oxygen adsorption r_a and oxygen incorporation r_i was performed. Fraction α, calculated from PIE measurements, was analysed by using the isotope kinetic equations [36]. Fig. 5a shows Arrhenius plots of the oxygen heterogenous surface exchange rate (r_H), the oxygen adsorption reaction rate (r_a) and the incorporation reaction rate (r_i) at each temperature. The surface exchange rate parameter r_H describes the isotope redistribution between the gas phase and oxide material. The exchange reaction process involves a sequence of reaction steps including adsorption, dissociation, charge transfer and incorporation of oxygen into the oxide lattice (with possible intermediates of O_2^-, O_2^{2-} or O^-). Each of these single steps can determine the oxygen heterogenous exchange rate [35]. The oxygen heterogeneous exchange rate is connected with the rates of oxygen dissociative adsorption and incorporation, according to the following equation:

$$r_H = r_a \bullet r_i / (r_a + r_i) \quad (5)$$

Analysis of the results carried out in the temperature-programmed mode, allowed calculation of surface activity parameters. The surface exchange corresponds to the surface exchange coefficient $k = r_H/C_O$, where C_O is the concentration of oxygen in the oxide. This approach allowed the description of the obtained data depending on the rates of oxygen dissociative adsorption (r_a) and oxygen incorporation (r_i).

The ratio between factors r_H:r_a:r_i was stable in the tested temperature range for $La_2NiO_{4+\delta}$ and $La_4Ni_3O_{10-\delta}$ and was almost independent of temperature. Therefore, the amount of incorporated oxygen was independent of temperature. This also confirmed high thermal stability in the tested temperature range. However, for $La_3Ni_2O_{7-\delta}$ in the temperature range 500–550 °C, the difference between the rates of oxygen dissociative adsorption and oxygen incorporation was slightly higher, which was reflected by the formation of a high amount of $^{16}O^{18}O$ in the gaseous phase during PIE tests. The gradient of the temperature dependency curves for $La_2NiO_{4+\delta}$ was higher than for $La_3Ni_2O_{7-\delta}$ or $La_4Ni_3O_{10-\delta}$ (Fig. 5a) indicating higher dependency of oxygen surface exchange properties on temperature. All oxygen kinetic parameters increased with temperature for all samples as expected. The difference in the heterogenous exchange rate between samples was relatively low. However, the highest r_H factor was for $La_3Ni_2O_{7-\delta}$ across the tested temperature range. At temperatures below 525 °C, the r_H rate was $La_2NiO_{4+\delta} > La_4Ni_3O_{10-\delta}$, and above the 525 °C it was the opposite ($La_4Ni_3O_{10-\delta} > La_2NiO_{4+\delta}$).

In the tested temperature range, the oxygen incorporation rate was found to be smaller than the rate of oxygen dissociative adsorption for $La_3Ni_2O_{7-\delta}$ and $La_4Ni_3O_{10-\delta}$ but not for $La_2NiO_{4+\delta}$. Therefore, the rate-determining step for $La_3Ni_2O_{7-\delta}$ and $La_4Ni_3O_{10-\delta}$ was oxygen incorporation. In contrast, dissociative adsorption of oxygen was rate-determining for $La_2NiO_{4+\delta}$. The difference between r_a and r_i was much smaller for $La_4Ni_3O_{10+\delta}$ compared to $La_3Ni_2O_{7+\delta}$ and $La_2NiO_{4+\delta}$, suggesting that for $La_4Ni_3O_{10+\delta}$ those two steps were partially competing in oxygen exchange rate determination. For $La_2NiO_{4+\delta}$, r_i was one order of magnitude higher than the r_a. The measured exchange rate for $La_2NiO_{4+\delta}$ was in good agreement with data reported in the literature [16,20,35,55]. For

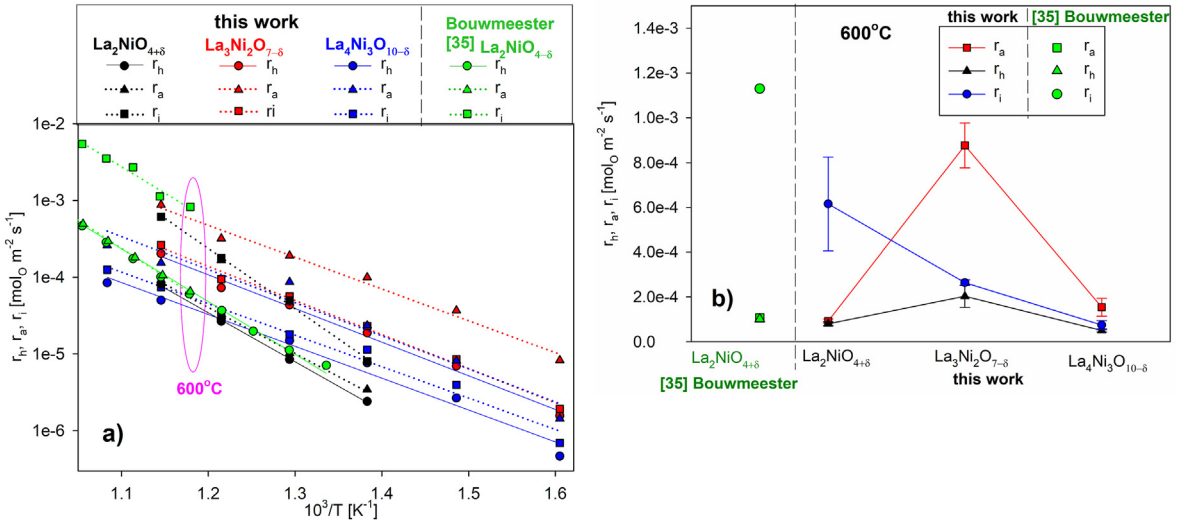

Fig. 5. a) Temperature dependencies of oxygen surface exchange rates; oxygen dissociative adsorption (r_a), incorporation (r_i) and oxygen heterogenous surface exchange rate (r_H) for lanthanum nickelates; b) the dependence of r_H, r_i, r_a parameters for Ruddlesden-Popper series of lanthanum nickelates, at 600 °C; and for $La_2NiO_{4+\delta}$ from literature [35].

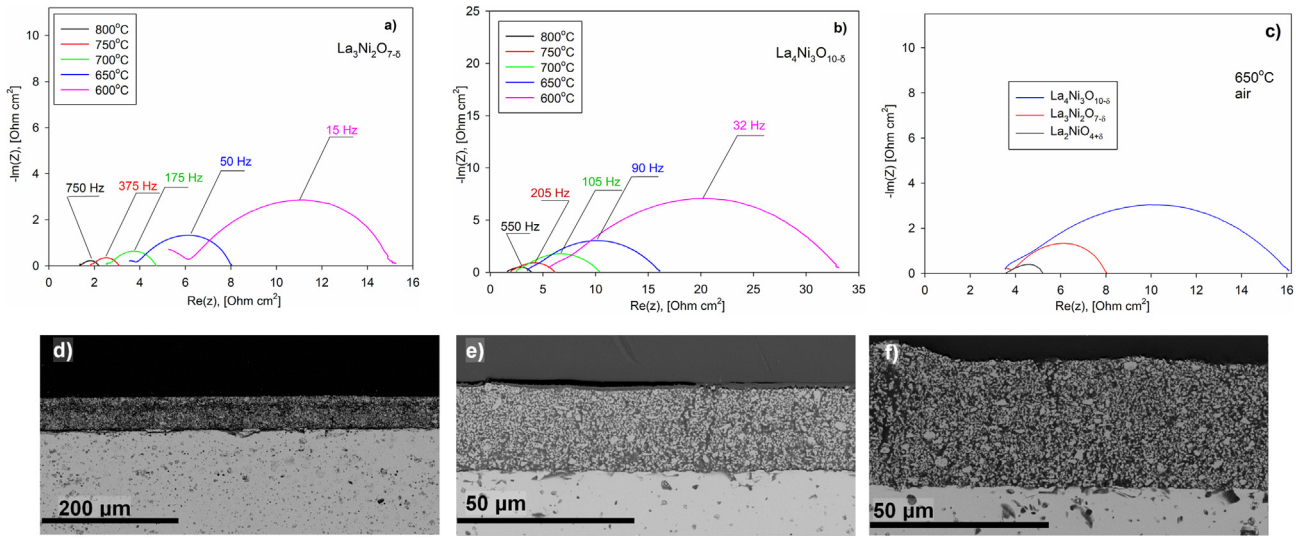

Fig. 6. Impedance spectra for the symmetric cells supported by $Ce_{0.8}Sm_{0.2}O_{1.9}$ electrolyte with electrodes: (a) $La_3Ni_2O_{7-\delta}$, (b) $La_4Ni_3O_{10-\delta}$ and (c) comparison at 650 °C for $La_{n+1}Ni_nO_{3n+1}$ ($n = 1$, 2 and 3) electrodes in dry air. Cross sections of tested electrodes: (d) $La_2NiO_{4+\delta}$, (e) $La_3Ni_2O_{7-\delta}$ and (f) $La_4Ni_3O_{10-\delta}$.

$La_2NiO_{4+\delta}$, the observed r_h and r_a (Fig. 5) were the same as reported by Bouwmeester [35] and the difference in r_i can be attributed to the error in r_i calculation and to differences in measurement technique, samples microstructure and thermal history. It should be also mentioned that r_H and r_a were determined independently from the experiment with their own measurement errors, while the value for r_i was calculated from equation (5).

Lou et al. [5], using the exchange current density calculations with EIS, also reported that for $La_4Ni_3O_{10-\delta}$ the oxygen diffusion process was rate-determining for the oxygen reduction reaction. This can be rationalised by the limitation of oxygen incorporation stemming from diffusion of the ^{16}O isotope from the bulk to the surface in order to interact with ^{18}O-labelled adatoms in the adsorption layer. The interrelation between the oxygen incorporation and diffusivity was shown for many oxides: $La_{1-x}Sr_xCoO_{3-\delta}$ [56], barium and calcium based zirconates [54], and lanthanum zirconates [57]. From Electrical Conductivity Relaxation (ECR) for oxygen transport properties, it was reported [25] that the surface exchange coefficient k_{chem} was similar for all LNOs. This observation is in corelation to the oxygen heterogenous surface exchange rate (r_H) (Fig. 5). However, the chemical diffusion coefficient D_{chem} was reported to decrease with increase in n parameter in $La_{n+1}Ni_nO_{3n+1}$. The authors concluded that oxygen diffusion strongly depends on the concentration of oxygen interstitial that is higher for hypo-stoichiometric $La_2NiO_{4+\delta}$.

Apparent activation energies were calculated from the r_H factor versus temperature. The activation energy for the LNO compounds was as follows; $La_2NiO_{4+\delta}$ 1.21 ± 0.06 eV, $La_3Ni_2O_{7-\delta}$ 0.81 ± 0.04 eV and $La_4Ni_3O_{10-\delta}$ 0.76 ± 0.05 eV. The activation energy thus decreased in the series $La_2NiO_{4+\delta} > La_3Ni_2O_{7-\delta} \sim La_4Ni_3O_{10-\delta}$, i.e., showing decreasing activation energy with increasing n.

The trend of r_i decreasing with the composition of a sample can be seen from Fig. 5b. The oxygen incorporation reaction rate (r_i) decreased with increasing Ni:O ratio and increasing n in $La_{n+1}Ni_nO_{3n+1}$ in the layered R–P structure. Therefore, the rate of the oxygen incorporation step r_i was directly connected to the R–P oxide structure. However, the oxygen dissociative adsorption *rate* and the oxygen heterogenous surface exchange rate were maximised in $La_3Ni_2O_{7-\delta}$. Therefore, we suggest that the r_i value depends on the structure of the lanthanum nickelate oxides, while r_a may vary and is not correlated with oxygen transport properties in the bulk.

A reduction in the number of oxygen stoichiometry presented by TGA (Fig. 1), was in correlation with the rate of oxygen incorporation (Fig. 5b). The results, therefore, suggest a relationship between $[O_i]$ and r_i. The oxygen nonstoichiometry in the tested LNOs varied with the Ni:O ratio in the lattice due to differing changes in the nickel oxidation state. The obtained results show a relationship between the oxygen non-stoichiometry and the oxygen incorporation rate for the tested LNOs. However, it is unlikely that the decrease in $[O_i]$ by the change in Ni content was solely responsible for the decrease in r_i. Probably, the decrease of r_i with n can be explained by the decrease in oxygen diffusivity. Unfortunately, it was not possible to extract the oxygen diffusion coefficient from the PIE data. It is also possible that these findings correlate with the surface structure and grain orientation of LNOs. The higher-order RPs are highly anisotropic. However, despite the broad discussion of oxygen vacancy migration in RP materials, anisotropy of the migration process needs further research to evaluate how surfaces orientation affects powder samples.

It was reported [16,37,57,58] that the dissociative oxygen adsorption rate depends on the defect structure within the outermost layer of the oxide. The low energy ion scattering results showed that the composition of the outermost layer of $La_2NiO_{4+\delta}$ is different than for $La_3Ni_2O_{7-\delta}$ and for $La_4Ni_3O_{10}$. Du to segregation of La ions and restructuring of the near-surface region Ni is absent in the outermost layer of $La_2NiO_{4+\delta}$ in comparison with $La_3Ni_2O_{7-\delta}$ and $La_4Ni_3O_{10-\delta}$. This result correlates with different rate-determining steps for $La_2NiO_{4+\delta}$ (oxygen dissociative adsorption limited) in comparison with $La_3Ni_2O_{7-\delta}$ and $La_4Ni_3O_{10-\delta}$ (oxygen incorporation limited). Obviously, the absence in the outermost layer of Ni as 3d-cation, which is preferable for the oxygen adsorption [59], makes the dissociative adsorption step on La cations rate-determining for $La_2NiO_{4+\delta}$. In contrast, the higher concentration of Ni in the outermost layer for $La_3Ni_2O_{7-\delta}$ gives a drastic increase in the oxygen dissociative adsorption rate. Segregation processes influenced by the composition of the outermost layer of $La_4Ni_3O_{10-\delta}$ lead to a decrease in r_a from $n = 2$ to $n = 3$.

3.3. EIS analysis of electrode kinetics for $La_{n+1}Ni_nO_{3n+1}$ ($n = 1$, 2 and 3) electrodes in contact with $Ce_{0.8}Sm_{0.2}O_{1.9}$ electrolyte

The suitability of LNOs for application as IT-SOC oxygen electrodes was investigated by impedance spectroscopy. The symmetrical cells were fired at 1,100 °C for 1 h to form oxygen electrodes. The EIS analyses for the electrodes made from the LNO powders with the cerium dioxide-based electrolyte tested in air in the temperature range 600–800 °C, are presented in Figs. 6 and 7. Fig. 6d–f shows micrographs of cell cross sections with a highly porous LNO oxygen electrode layer deposited on a dense $Ce_{0.8}Sm_{0.2}O_{1.9}$ electrolyte after the completion of all testing. The

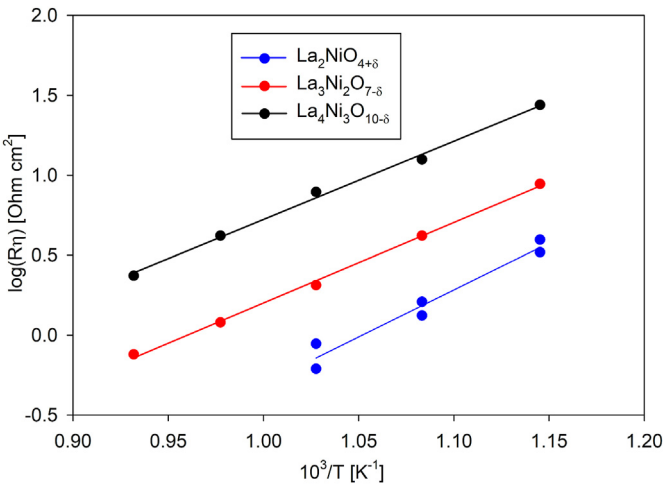

Fig. 7. Temperature dependence of polarisation resistance for $La_{n+1}Ni_nO_{3n+1}$ (n = 1, 2 and 3) electrodes in contact with CeO_2-based electrolyte with temperature.

electrode layers were of 25–45 μm thickness and exhibited a porous, evenly distributed microstructure.

The impedance spectra were analysed for the tested symmetrical cells as a function of temperature, with Nyquist plots presented in Fig. 6a and b for $La_3Ni_2O_{7-\delta}$ and $La_4Ni_3O_{10-\delta}$, respectively. The values of the polarisation resistance were calculated as the difference between the values of the low-frequency intercept with the real axis and the minimum at the high-frequency region of the impedance spectrum. The relationship has the following form, considering the geometry of the electrodes:

$$R_\eta = \frac{(R_{dc} - R_s) \cdot S}{2} \quad (6)$$

where R_η is the polarisation resistance, S is the electrode area, R_{dc} is the cell resistance to direct current, and R_s is the high-frequency resistance, which corresponds to the apparent ohmic resistance of the electrolyte. The apparent ohmic resistance of the electrolyte decreased with an increase in temperature. Also, the symmetrical cell polarisation resistance decreased with increasing temperature (Fig. 6a and b). The asymmetric shape for all spectra suggested an electrode processes consisting of several steps. With an increase in the temperature from 600 to 800 °C, the obtained spectra shifted towards lower values. That change was most likely due to the enhancement in the electrodes' ionic conductivity and surface reaction kinetics. The observed polarisation resistance was slightly higher than that reported in the literature [24], and this can be attributed to the adhesion between electrodes and the electrolyte components. The applied sintering temperature of 1,100 °C was probably too low to obtain good adhesion of the electrodes to the electrolyte surface. The application of an intermediate mixed electrode/electrolyte layer could also improve this adhesion. For $La_2NiO_{4+\delta}$ symmetrical cells, the impedance data were reported [20] to be dominated by Gerischer-type dispersion. The shape of dispersion for $La_2NiO_{4+\delta}$ in Fig. 6c (black) confirmed that observation. For $La_3Ni_2O_{7-\delta}$ and $La_4Ni_3O_{10-\delta}$ electrodes, the dispersion shape was different (Fig. 6c red/blue) and can be retrieved by low frequency (RQ)-type dispersion.

The comparison of the polarisation resistance for $La_3Ni_2O_{7-\delta}$ and $La_4Ni_3O_{10-\delta}$ electrodes in contact with the CeO_2-based electrolyte data for the $La_2NiO_{4+\delta}$ electrode in air conditions, at 700 °C is presented in Fig. 7.

The values of polarisation resistance increase in the sequence $La_2NiO_{4+\delta} < La_3Ni_2O_{7-\delta} < La_4Ni_3O_{10-\delta}$, and, therefore, the best performance was obtained for the $La_2NiO_{4+\delta}$ electrode. This is in correlation to the reported [25] oxygen self-diffusion coefficients for $La_{n+1}NinO_{3n+1}$ which decrease with n parameter. The polarisation resistance (Fig. 6) increased with the increase in the n value for $La_{n+1}Ni_nO_{3n+1}$ and the differences seemed independent of temperature in the tested range. This suggests that changes in gas diffusion and the oxygen exchange on the electrode surface had a similar rate for all tested LNO samples with the increase in temperature. The lower polarisation resistance for $La_2NiO_{4+\delta}$ is attributed to the presence of a high amount of interstitial oxygen in its structure and the lower barrier for oxyanion transport, despite the reported lower overall electronic conductivity. This reveals that diffusion of oxide ions from the surface to the bulk is a key limiting step for LNO electrodes.

Arrhenius plots (Fig. 7) for the reciprocal polarisation resistance R_η show the correlation of polarisation resistance with temperature, with minimal values for $La_2NiO_{4+\delta}$. The polarisation resistance was 0.44, 1.31 and 5.09 Ohm cm^2 at 700 °C for $La_2NiO_{4+\delta}$, $La_3Ni_2O_{7-\delta}$, $La_4Ni_3O_{10-\delta}$, respectively. However, the lowest activation energy of the polarisation conductivity ($1/R_h$) was 102 kJ mol^{-1} for $La_3Ni_2O_{7-\delta}$. The obtained activation energy measurements corresponded to the overall surface exchange rate (r_H) data from oxygen exchange rate studies (Fig. 5b).

The difference in EIS spectra for the $La_2NiO_{4+\delta}$ electrode in comparison with $La_3Ni_2O_{7-\delta}$ and $La_4Ni_3O_{10-\delta}$ (Fig. 6c), could indicate that the mechanism of electrode reaction was different for these two cases. This coincided with the PIE r_i and r_a analyses: oxygen dissociative adsorption limited kinetics for $La_2NiO_{4+\delta}$, and oxygen incorporation was the limiting step for $La_3Ni_2O_{7-\delta}$ and $La_4Ni_3O_{10-\delta}$ oxides.

A decrease of the electrode activity in the series with n correlates strongly with a decrease of the oxygen incorporation measured by PIE. Taking into account that the lower polarisation resistance for $La_2NiO_{4+\delta}$, is attributed to the presence of a high amount of interstitial oxygen in its structure and the lower barrier for the interstitial oxygen transport, one can conclude the observed connection between the high oxygen mobility, high oxygen incorporation rate and low polarisation resistance. For the $La_2NiO_{4+\delta}$ phase, migration of oxygen atoms can probably have a cooperative mechanism with regular oxygen vacancy pathways in the Perovskite layer and movement of weakly bound oxygen on interstitial positions in the rock salt layer, whereas for $La_3Ni_2O_{7-\delta}$ and $La_4Ni_3O_{10-\delta}$, oxygen migration is limited mostly to oxygen vacancies with slower oxygen diffusivity within the Perovskite layers.

3.4. Ruddlesden-Popper structure and electrode performance

The oxygen kinetic properties and the electrical properties are responsible for the overall oxygen electrode performance. Especially the electrochemical performance of a mixed conductor electrode is affected by oxygen exchange properties and oxygen migration. All the available literature reports confirm the increase in the LNO overall conductivity with an increase in n, as a result of higher electronic conductivity. The conductivity in $La_{n+1}Ni_nO_{3n+1}$ depends on the valence of the Ni ion (Ni^{3+}>Ni^{2+}), the number of the Perovskite layers and the oxygen content. Since the LNO charge carrier transport takes place mostly in the equatorial planes of the NiO_6 octahedra, the electronic conductivity increases with an increase in the number of Perovskite layers.

However, the obtained electrochemical activity results of the electrodes indicated higher activity of the $La_2NiO_{4+\delta}$ electrode compared to the $La_3Ni_2O_{7-\delta}$ or $La_4Ni_3O_{10-\delta}$ electrodes. $La_2NiO_{4+\delta}$ with oxygen non-stoichiometry due to interstitial oxygen showed lower polarisation resistance than LNO phases with oxygen deficiency. Thus, the polarisation resistance for the tested LNO samples, was found to follow a different trend to the oxygen surface exchange properties. In particular, the tested LNO materials that showed high surface activity, showed also high polarisation resistance. $La_2NiO_{4+\delta}$, despite having the lowest thermally activated oxygen dissociative adsorption rate, showed the highest electrochemical activity among those investigated materials. Improved surface oxygen activity, therefore, had no positive effect on the overall electrochemical performance. However, there is a correlation between the LNO samples' polarisation resistance and the oxygen incorporation rate. Therefore, it can be concluded that the electrochemical performance

of the tested electrodes depends on the oxygen incorporation activity.

Lattice defects with oxygen nonstoichiometry in a lattice structure are responsible for oxygen incorporation (Eq. (2)), therefore, the rate of oxygen incorporation depends on the migration of nonstoichiometric oxygen, i.e. oxygen vacancies or interstitials. For $La_2NiO_{4+\delta}$ it has been reported that there is an accumulation of highly mobile interstitial oxygen in $La_2O_{2+\delta}$ layers, with oxygen vacancies that exist in $LaNiO_{3-\delta}$ Perovskite regions. Therefore, fast oxygen migration via two mechanisms is possible, and the existence of two channels of oxygen migration in these nickelates was recently reported via a cooperative mechanism. The layered structure of $La_2NiO_{4+\delta}$ that allows for two-channel migration can be responsible for the observed good electrochemical performance, despite the lower surface activity. For $La_2NiO_{4+\delta}$, the mechanism involving the interstitial oxygen dominates oxygen diffusion. The observed lower oxygen incorporation rate for $La_3Ni_2O_{7-\delta}$ or $La_4Ni_3O_{10-\delta}$ compared to $La_2NiO_{4+\delta}$ was probably caused by a lack of highly mobile interstitial oxygen, as confirmed by TGA results, which rather suggests the presence of oxide ion vacancies. The results of high surface activity and low electrochemical performance for higher-order R–P can be explained by the surface exchange that led to the formation of surface oxygen adatoms but did not result in high oxygen diffusion. Also, the LNOs' anisotropic structure and the 2-D ionic conductivity affected the performance of electrodes. Cells' microstructure also could be responsible for lower electrochemical performance. Due to material instability, the tested electrodes were sintered at relatively low temperature resulting in reduced adherence to the electrolyte and consequently in inadequately defined TPB. Therefore, charge transfer in the TPB layer could limit cells' electrochemical performance. An additional dense base-layer between the porous electrode and an electrolyte was reported [20] to improve the TPB region for electrodes with oxygen surface diffusion properties.

The absence of Ni in the outermost crystallographic surface for $Ln_2NiO_{4+\delta}$ resulted in a low oxygen dissociative adsorption rate. The fact that the sites that interact with gaseous oxygen and are active for catalytic oxygen reduction are hidden below the La-enriched atomic surface layer therefore affected the oxygen adsorption properties. The overall exchange reaction at the gas/surface interface involves the formation of electron holes:

$$\frac{1}{2}O_2 \leftrightarrow O_i'' + 2\dot{h} \tag{7}$$

$$\frac{1}{2}O_2 + V_O^{\cdot\cdot} \leftrightarrow O_O^x + 2\dot{h} \tag{8}$$

The process involves a charge transfer step that usually is caused by the oxidation of B-site cations. However, if Ni is not present on the surface, the oxygen adsorption process is restrained. Despite the lower oxygen adsorption rate, $La_2NiO_{4+\delta}$ has relatively high catalytic activity in oxygen reduction. The role of A-site cations in promoting charge transfer to surface adsorbates on the A-O terminated surface was explained by Akbay et al. [60]. The performance of an SOC oxygen electrode is related not only to the electrical conductivity but also to the electrode microstructure. Therefore, the reported literature differences in ASR can be related to differences in cell microstructure. These variations in observed LNO performance are probably a result of the reported difficulty in sintering those R–P higher order phases [30,33]. The proportion between low and high-frequency resistance response and the overall polarisation resistance for LNOs was reported to depend on microstructure [9]. Additionally, oxygen diffusion through the LNO crystal structure is anisotropic [12,61,62]. The oxygen incorporation stage was reported to depend on the grain primary orientation [16]. Authors reported that materials with grains' primary orientation along the *c*-axis have a negligible incorporation rate that limits the oxygen surface exchange process. While for grains with the (*ab*)-crystallographic orientation, dissociative adsorption is the rate-determining stage. For $Ln_2NiO_{4+\delta}$ rare-earth nickelate oxygen diffusion within the (*ab*)-plane was reported to be three orders of magnitude higher compared to the c-axis direction [49,62]. For those polycrystalline materials, the oxygen exchange process in the (*ab*)-plane direction is dominating, as the crystallographic orientation with the highest surface exchange coefficient. However, the influence of surface inhomogeneity on oxygen exchange kinetics for the higher-order R–P structures needs further research. Also, the tested polycrystalline ceramic samples contained a range of grains with random orientation resulting in median surface properties. Therefore, for R–P structures, oxygen diffusion depends on the connectivity between grains. Hildenbrand et al. [20], based on a two-step oxygen exchange mechanism suggested that surface diffusion can dominate the oxygen transport path for porous $La_2NiO_{4+\delta}$. The tentative model suggests that oxygen adsorbs dissociatively on the $La_2NiO_{4+\delta}$ surface forming mobile O^-_{ad} species responsible for surface diffusion of monoatomic oxygen as a major transport path.

The tested materials $La_2NiO_{4+\delta}$, $La_3Ni_2O_{7-\delta}$ and $La_4Ni_3O_{10-\delta}$ are all considered as promising candidates for application as high-performance oxygen electrodes for intermediate-temperature SOC (IT-SOC). However, the presented comparisons suggest that the $La_2NiO_{4+\delta}$ electrode has more potential for application in the IT-SOC than $La_3Ni_2O_{7-\delta}$ or $La_4Ni_3O_{10-\delta}$. However, given reports of low $La_2NiO_{4+\delta}$ stability, mixing the electrode material with both $La_3Ni_2O_{7-\delta}$ or $La_4Ni_3O_{10-\delta}$ could improve electronic conductivity and overall electrode performance. Also, preparing $La_3Ni_2O_{7-\delta}$ and $La_4Ni_3O_{10-\delta}$ composite electrode with an ionic conductor (electrolyte material) or with $La_2NiO_{4+\delta}$ within the electrode functional layer could improve the overall cell performance by improving ionic conductivity and overall electrochemical activity. Furthermore, some A-site substitution could potentially improve oxygen mobility in $La_3Ni_2O_{7-\delta}$ and $La_4Ni_3O_{10-\delta}$ structures by increase of oxygen deficiency and thus enhance the oxide ion diffusivity and facilitate oxygen migration in those RP oxides. For example, substitution of an aliovalent cations for La^{3+} on the A site can lead to the formation of defects with charge compensation by either electron holes or oxygen vacancies.

4. Conclusions

$La_2NiO_{4+\delta}$, $La_3Ni_2O_{7-\delta}$ and $La_4Ni_3O_{10-\delta}$ oxide materials were comprehensively studied for their application in IT-SOCs. These LNO phases were studied using the technique of temperature-programmed pulse isotope exchange of oxygen with $^{18}O_2$ in a flow reactor. The obtained results confirmed the high oxygen surface exchange rate for these oxides.

PIE analysis showed that the oxygen surface exchange rate for $La_2NiO_{4+\delta}$ was limited by the rate of dissociative adsorption of oxygen molecules at the oxide surface. In contrast, this oxygen adsorption was more facile for $La_3Ni_2O_{7-\delta}$ and $La_4Ni_3O_{10-\delta}$, and in these cases, the limiting process was the oxygen incorporation rate. The difference in the rate-determining step of for $La_2NiO_{4+\delta}$ in comparison with $La_3Ni_2O_{7-\delta}$ and $La_4Ni_3O_{10-\delta}$ is caused by the different defect chemistry of the outermost layer. LEIS results showed higher oxygen concentration for $n = 1$ and the absence in the outermost layer of Ni, which is preferable for the oxygen adsorption in comparison with La–O terminated surfaces, which makes dissociative adsorption step on La cations rate-determining for $La_2NiO_{4+\delta}$. The absence of Ni in the outermost layer of powdered $La_2NiO_{4+\delta}$, agrees with similar results obtained previously on single crystals and polycrystalline materials in the literature. The increase in polarisation resistance for $La_{n+1}Ni_nO_{3n+1}$ with n correlates with the decrease in the oxygen incorporation rate and also with the increase in the Ni concentration and the decrease in the oxygen concentration in the outermost layer.

In terms of electrode performance, $La_2NiO_{4+\delta}$ had the lowest level of polarisation resistance in addition to an excellent oxygen incorporation rate. The higher-order R–P structures such as $La_3Ni_2O_{7-\delta}$ and $La_4Ni_3O_{10-\delta}$ had a higher surface activity and oxygen dissociative adsorption rate but low oxygen incorporation rate and a high polarisation resistance. Correlation between the electrochemical performance and surface oxygen activity and electrode structure was demonstrated. The polarisation

resistance of the tested LNO electrodes was found to correlate with the rate of oxygen adatom incorporation into the crystal structure of the oxide, which is limited by the oxygen diffusivity. Thus, for improvement in the performance of $n = 2$, 3 phases, higher oxide ion conductivity is needed. This may potentially be achieved by incorporation of higher valent dopants to move the compositions into the oxygen interstitial region, or by the use of a composite electrode with the electrolyte material.

The results herein suggest that all the tested electrodes hold promise for use in IT-SOCs, with further work warranted in particular in terms of use of doped or composite electrodes.

Conflicts of interest

There are no conflicts to declare.

CRediT authorship contribution statement

Artur J. Majewski: Writing – original draft, Conceptualization, Investigation. **Anna Khodimchuk:** Investigation, Formal analysis. **Dmitriy Zakharov:** Data curation, Formal analysis. **Natalia Porotnikova:** Formal analysis. **Maxim Ananyev:** Methodology, Formal analysis, Conceptualization. **Ian D. Johnson:** Resources, Validation. **Jawwad A. Darr:** Resources, Writing – review & editing. **Peter R. Slater:** Supervision, Funding acquisition, Writing – review & editing. **Robert Steinberger-Wilckens:** Supervision, Writing – review & editing.

Declaration of competing interest

The authors declare that they have no known competing financial interests or personal relationships that could have appeared to influence the work reported in this paper.

Acknowledgements

The authors would like to express their appreciation to EPSRC, UK for support through the JUICED Hub (contract EP/R023662/1) funding. LEIS data collection was performed at the EPSRC National Facility for XPS (HarwellXPS).

Appendix A. Supplementary data

Supplementary data to this article can be found online at https://doi.org/10.1016/j.jssc.2022.123228.

References

[1] R.K. Sharma, E. Djurado, Functionally graded and homogeneous composites of $La_2NiO_{4+\delta}$ and $La_{n+1}Ni_nO_{3n+1}$ (n = 2 and 3) solid oxide fuel cell cathodes, J. Mater. Chem. 5 (42) (2017) 22277–22287.

[2] S. Choi, S. Yoo, J.-Y. Shin, G. Kim, High performance SOFC cathode prepared by infiltration of $la_{n+1}Ni_nO_{3n+1}$ (n = 1, 2, and 3) in porous YSZ, J. Electrochem. Soc. 158 (8) (2011) B995.

[3] G. Amow, I.J. Davidson, S.J. Skinner, A comparative study of the Ruddlesden-Popper series, $La_{n+1}Ni_nO_{3n+1}$ (n=1, 2 and 3), for solid-oxide fuel-cell cathode applications, Solid State Ionics 177 (13) (2006) 1205–1210.

[4] S. Takahashi, S. Nishimoto, M. Matsuda, M. Miyake, Electrode properties of the ruddlesden–popper series, $La_{n+1}Ni_nO_{3n+1}$ (n=1, 2, and 3), as intermediate-temperature solid oxide fuel cells, J. Am. Ceram. Soc. 93 (8) (2010) 2329–2333.

[5] Z. Lou, N. Dai, Z. Wang, Y. Dai, Y. Yan, J. Qiao, J. Peng, J. Wang, K. Sun, Preparation and electrochemical characterization of Ruddlesden–Popper oxide $La_4Ni_3O_{10}$ cathode for IT-SOFCs by sol–gel method, J. Solid State Electrochem. 17 (10) (2013) 2703–2709.

[6] B. Koo, K. Kim, J.K. Kim, H. Kwon, J.W. Han, W. Jung, Sr segregation in perovskite oxides: why it happens and how it exists, Joule 2 (8) (2018) 1476–1499.

[7] D.K. Seo, W. Liang, M.H. Whangbo, Z. Zhang, M. Greenblatt, Electronic band structure and madelung potential study of the nickelates La_2NiO_4, $La_3Ni_2O_7$, and $La_4Ni_3O_{10}$, Inorg. Chem. 35 (22) (1996) 6396–6400.

[8] R.J. Woolley, B.N. Illy, M.P. Ryan, S.J. Skinner, In situ determination of the nickel oxidation state in $La_2NiO_{4+\delta}$ and $La_4Ni_3O_{10-\delta}$ using X-ray absorption near-edge structure, J. Mater. Chem. 21 (46) (2011) 18592–18596.

[9] R.K. Sharma, M. Burriel, E. Djurado, $La_4Ni_3O_{10-\delta}$ as an efficient solid oxide fuel cell cathode: electrochemical properties versus microstructure, J. Mater. Chem. 3 (47) (2015) 23833–23843.

[10] E. Tropin, M. Ananyev, N. Porotnikova, A. Khodimchuk, S. Saher, A. Farlenkov, E. Kurumchin, D. Shepel, E. Antipov, S. Istomin, H. Bouwmeester, Oxygen surface exchange and diffusion in $Pr_{1.75}Sr_{0.25}Ni_{0.75}Co_{0.25}O_{4\pm\delta}$, Phys. Chem. Chem. Phys. 21 (9) (2019) 4779–4790.

[11] S.J. Skinner, J.A. Kilner, Oxygen diffusion and surface exchange in $La_{2-x}Sr_xNiO_{4+\delta}$, Solid State Ionics 135 (1) (2000) 709–712.

[12] J.M. Bassat, P. Odier, A. Villesuzanne, C. Marin, M. Pouchard, Anisotropic ionic transport properties in $La_2NiO_{4+\delta}$ single crystals, Solid State Ionics 167 (3) (2004) 341–347.

[13] X. Tong, F. Zhou, S. Yang, S. Zhong, M. Wei, Y. Liu, Performance and stability of Ruddlesden-Popper $La_2NiO_{4+\delta}$ oxygen electrodes under solid oxide electrolysis cell operation conditions, Ceram. Int. 43 (14) (2017) 10927–10933.

[14] J.D. Jorgensen, B. Dabrowski, S. Pei, D.R. Richards, D.G. Hinks, Structure of the interstitial oxygen defect in La_2NiO_{4+d}, Phys. Rev. B 40 (4) (1989) 2187–2199.

[15] L. Minervini, R.W. Grimes, J.A. Kilner, K.E. Sickafus, Oxygen migration in LaNiO, J. Mater. Chem. 10 (10) (2000) 2349–2354.

[16] M.V. Ananyev, E.S. Tropin, V.A. Eremin, A.S. Farlenkov, A.S. Smirnov, A.A. Kolchugin, N.M. Porotnikova, A.V. Khodimchuk, A.V. Berenov, E.K. Kurumchin, Oxygen isotope exchange in $La_2NiO_{4\pm\delta}$, Phys. Chem. Chem. Phys. 18 (13) (2016) 9102–9111.

[17] M.V. Ananyev, D.I. Bronin, D.A. Osinkin, V.A. Eremin, R. Steinberger-Wilckens, L.G.J. de Haart, J. Mertens, Characterization of Ni-cermet degradation phenomena I. Long term resistivity monitoring, image processing and X-ray fluorescence analysis, J. Power Sources 286 (2015) 414–426.

[18] A. Montenegro-Hernández, J. Vega-Castillo, L. Mogni, A. Caneiro, Thermal stability of $Ln_2NiO_{4+\delta}$ (Ln: La, Pr, Nd) and their chemical compatibility with YSZ and CGO solid electrolytes, Int. J. Hydrogen Energy 36 (24) (2011) 15704–15714.

[19] Y. Lee, H. Kim, Electrochemical performance of $La_2NiO_{4+\delta}$ cathode for intermediate-temperature solid oxide fuel cells, Ceram. Int. 41 (4) (2015) 5984–5991.

[20] N. Hildenbrand, P. Nammensma, D.H.A. Blank, H.J.M. Bouwmeester, B.A. Boukamp, Influence of configuration and microstructure on performance of $La_2NiO_{4+\delta}$ intermediate-temperature solid oxide fuel cells cathodes, J. Power Sources 238 (2013) 442–453.

[21] J. Railsback, S.A. Barnett, Performance and stability of La_2NiO_4-infiltrated $La_{0.9}Sr_{0.1}Ga_{0.8}Mg_{0.2}O_3$ oxygen electrodes during current switched life testing, J. Power Sources 395 (2018) 1–7.

[22] A.A. Kol'chugin, E.Y. Pikalova, N.M. Bogdanovich, D.I. Bronin, E.A. Filonova, Electrochemical properties of doped lantanum–nickelate-based electrodes, Russ. J. Electrochem. 53 (8) (2017) 826–833.

[23] V.A. Sadykov, E.M. Sadovskaya, E.Y. Pikalova, A.A. Kolchugin, E.A. Filonova, S.M. Pikalov, N.F. Eremeev, A.V. Ishchenko, A.I. Lukashevich, J.M. Bassat, Transport features in layered nickelates: correlation between structure, oxygen diffusion, electrical and electrochemical properties, Ionics 24 (4) (2018) 1181–1193.

[24] R.K. Sharma, M. Burriel, L. Dessemond, J.-M. Bassat, E. Djurado, $La_{n+1}Ni_nO_{3n+1}$ (n = 2 and 3) phases and composites for solid oxide fuel cell cathodes: facile synthesis and electrochemical properties, J. Power Sources 325 (2016) 337–345.

[25] J. Song, D. Ning, B. Boukamp, J.-M. Bassat, H.J.M. Bouwmeester, Structure, electrical conductivity and oxygen transport properties of Ruddlesden–Popper phases $Ln_{n+1}Ni_nO_{3n+1}$ (Ln = La, Pr and Nd; n = 1, 2 and 3), J. Mater. Chem. 8 (42) (2020) 22206–22221.

[26] J. Yu, J. Sunarso, Y. Zhu, X. Xu, R. Ran, W. Zhou, Z. Shao, Activity and stability of ruddlesden–popper-type $La_{n+1}Ni_nO_{3n+1}$ (n=1, 2, 3, and ∞) electrocatalysts for oxygen reduction and evolution reactions in alkaline media, Chem. Eur J. 22 (8) (2016) 2719–2727.

[27] C.M. Harrison, P.R. Slater, R. Steinberger-Wilckens, The reactivity and stability of La-nickelate cathode materials, in: O. Bucheli, G. Geisser, F. Moore, M. Spirig (Eds.), 14th European SOFC & SOE Forum 2020, EFCF, Lucerne Switzerland, 2020, pp. 481–486.

[28] C.S. Ni, D.F. Zhang, C.Y. Ni, Z.M. Wang, Ruddlesden–Popper nickelate as coating for chromia-forming stainless steel, Int. J. Hydrogen Energy 39 (25) (2014) 13314–13319.

[29] V.R.M. Melo, R.L.B.A. Medeiros, R.M. Braga, H.P. Macedo, J.A.C. Ruiz, G.T. Moure, M.A.F. Melo, D.M.A. Melo, Study of the reactivity of Double-perovskite type oxide $La_{1-x}M_xNiO_4$ (M = Ca or Sr) for chemical looping hydrogen production, Int. J. Hydrogen Energy 43 (3) (2018) 1406–1414.

[30] R.J. Woolley, S.J. Skinner, Novel $La_2NiO_{4+\delta}$ and $La_4Ni_3O_{10-\delta}$ composites for solid oxide fuel cell cathodes, J. Power Sources 243 (2013) 790–795.

[31] X. Weng, P. Boldrin, I. Abrahams, S.J. Skinner, J.A. Darr, Direct syntheses of mixed ion and electronic conductors $La_4Ni_3O_{10}$ and $La_3Ni_2O_7$ from nanosized coprecipitates, Chem. Mater. 19 (18) (2007) 4382–4384.

[32] M. Zinkevich, F. Aldinger, Thermodynamic analysis of the ternary La–Ni–O system, J. Alloys Compd. 375 (1) (2004) 147–161.

[33] Y. Adachi, N. Hatada, K. Hirota, M. Kato, T. Uda, Preparation of pure and fully dense lanthanum nickelates $La_{n+1}Ni_nO_{3n+1}$ (n = 2, 3, ∞) by post-sintering oxidation process, J. Am. Ceram. Soc. 102 (12) (2019) 7077–7088.

[34] B.H. Toby, R.B. Von Dreele, GSAS-II: the genesis of a modern open-source all purpose crystallography software package, J. Appl. Crystallogr. 46 (2) (2013) 544–549.

[35] H.J.M. Bouwmeester, C. Song, J. Zhu, J. Yi, M. van Sint Annaland, B.A. Boukamp, A novel pulse isotopic exchange technique for rapid determination of the oxygen

surface exchange rate of oxide ion conductors, Phys. Chem. Chem. Phys. 11 (42) (2009) 9640–9643.
[36] G.K. Boreskov, V.S. Muzykantov, Investigation of oxide-type oxidation catalysts by reactions of oxygen isotopic exchange, Ann. N. Y. Acad. Sci. 213 (1) (1973) 137–170.
[37] M.V. Ananyev, V.A. Eremin, D.S. Tsvetkov, N.M. Porotnikova, A.S. Farlenkov, A.Y. Zuev, A.V. Fetisov, E.K. Kurumchin, Oxygen isotope exchange and diffusion in $LnBaCo_2O_{6-\delta}$ (Ln=Pr, Sm, Gd) with double perovskite structure, Solid State Ionics 304 (2017) 96–106.
[38] C.-Y. Yoo, B.A. Boukamp, H.J.M. Bouwmeester, Oxygen surface exchange kinetics on $PrBaCo_2O_{5+\delta}$, Solid State Ionics 262 (2014) 668–671.
[39] A.V. Khodimchuk, D.M. Zakharov, N.A. Shevyrev, A.S. Farlenkov, N.A. Zhuravlev, T.A. Denisova, M.V. Ananyev, $^{18}O/^{16}O$ isotope exchange for yttria stabilised zirconia in dry and humid oxygen, Int. J. Hydrogen Energy (2021).
[40] E.P. Antonova, A.V. Khodimchuk, G.R. Usov, E.S. Tropin, A.S. Farlenkov, A.V. Khrustov, M.V. Ananyev, EIS analysis of electrode kinetics for $La_2NiO_{4+\delta}$ cathode in contact with $Ce_{0.8}Sm_{0.2}O_{1.9}$ electrolyte: from DRT analysis to physical model of the electrochemical process, J. Solid State Electrochem. 23 (4) (2019) 1279–1287.
[41] V. Vibhu, A. Rougier, C. Nicollet, A. Flura, S. Fourcade, N. Penin, J.-C. Grenier, J.-M. Bassat, $Pr_4Ni_3O_{10+\delta}$: a new promising oxygen electrode material for solid oxide fuel cells, J. Power Sources 317 (2016) 184–193.
[42] E. Pikalova, A. Kolchugin, N. Bogdanovich, D. Medvedev, J. Lyagaeva, L. Vedmid, M. Ananyev, S. Plaksin, A. Farlenkov, Suitability of $Pr_{2-x}Ca_xNiO_{4+\delta}$ as cathode materials for electrochemical devices based on oxygen ion and proton conducting solid state electrolytes, Int. J. Hydrogen Energy 45 (25) (2020) 13612–13624.
[43] M. Deus Carvalho, F. Madalena, A. Costa, I. da Silva Pereira, A. Wattiaux, J. Marc Bassat, J. Claude Grenier, M. Pouchard, New preparation method of $La_{n+1}Ni_nO_{3n+1-\delta}$ (n=2, 3), J. Mater. Chem. 7 (10) (1997) 2107–2111.
[44] S.Y. Jeon, M.B. Choi, H.N. Im, J.H. Hwang, S.J. Song, Oxygen ionic conductivity of $La_2NiO_{4+\delta}$ via interstitial oxygen defect, J. Phys. Chem. Solid. 73 (5) (2012) 656–660.
[45] X. Weng, J.C. Knowles, I. Abrahams, Z. Wu, J.A. Darr, In situ variable temperature X-ray diffraction studies on the transformations of nano-precursors to La–Ni–O phases, J. Solid State Chem. 184 (7) (2011) 1688–1694.
[46] J. Wu, S.S. Pramana, S.J. Skinner, J.A. Kilner, A.P. Horsfield, Why Ni is absent from the surface of $La_2NiO_{4+\delta}$? J. Mater. Chem. 3 (47) (2015) 23760–23767.
[47] M. Burriel, S. Wilkins, J.P. Hill, M.A. Muñoz-Márquez, H.H. Brongersma, J.A. Kilner, M.P. Ryan, S.J. Skinner, Absence of Ni on the outer surface of Sr doped La_2NiO_4 single crystals, Energy Environ. Sci. 7 (1) (2014) 311–316.
[48] J. Druce, H. Téllez, M. Burriel, M.D. Sharp, L.J. Fawcett, S.N. Cook, D.S. McPhail, T. Ishihara, H.H. Brongersma, J.A. Kilner, Surface termination and subsurface restructuring of perovskite-based solid oxide electrode materials, Energy Environ. Sci. 7 (11) (2014) 3593–3599.
[49] M. Burriel, H. Téllez, R.J. Chater, R. Castaing, P. Veber, M. Zaghrioui, T. Ishihara, J.A. Kilner, J.-M. Bassat, Influence of crystal orientation and annealing on the oxygen diffusion and surface exchange of $La_2NiO_{4+\delta}$, J. Phys. Chem. C 120 (32) (2016) 17927–17938.
[50] K.T. Wu, H. Téllez, J. Druce, M. Burriel, F. Yang, D.W. McComb, T. Ishihara, J.A. Kilner, S.J. Skinner, Surface chemistry and restructuring in thin-film $La_{n+1}Ni_nO_{3n+1}$ (n = 1, 2 and 3) Ruddlesden–Popper oxides, J. Mater. Chem. 5 (19) (2017) 9003–9013.
[51] E.S. Tropin, M.V. Ananyev, A.S. Farlenkov, A.V. Khodimchuk, A.V. Berenov, A.V. Fetisov, V.A. Eremin, A.A. Kolchugin, Surface defect chemistry and oxygen exchange kinetics in $La_{2-x}Ca_xNiO_{4+\delta}$, J. Solid State Chem. 262 (2018) 199–213.
[52] C.-l. Song, J.-x. Yi, Y. Yan, Detailed description of pulse isotopic exchange method for analyzing oxygen surface exchange behavior on oxide ion conductors, Chin, J. Chem. Phys. 32 (4) (2019) 474–484.
[53] M.W. den Otter, B.A. Boukamp, H.J.M. Bouwmeester, Theory of oxygen isotope exchange, Solid State Ionics 139 (1) (2001) 89–94.
[54] A.S. Farlenkov, M.V. Ananyev, V.A. Eremin, N.M. Porotnikova, E.K. Kurumchin, B.T. Melekh, Oxygen isotope exchange in doped calcium and barium zirconates, Solid State Ionics 290 (2016) 108–115.
[55] E.P. Antonova, A.V. Khodimchuk, E.S. Tropin, N.M. Porotnikova, A.S. Farlenkov, M.I. Vlasov, M.V. Ananyev, Influence of modifying additives on electrochemical performance of $La_2NiO_{4+\delta}$ - based oxygen electrodes, Solid State Ionics 346 (2020) 115215.
[56] M.V. Ananyev, N.M. Porotnikova, E.K. Kurumchin, Influence of strontium content on the oxygen surface exchange kinetics and oxygen diffusion in $La_{1-x}Sr_xCoO_{3-\delta}$ oxides, Solid State Ionics 341 (2019) 115052.
[57] A.S. Farlenkov, A.V. Khodimchuk, V.A. Eremin, E.S. Tropin, A.V. Fetisov, N.A. Shevyrev, I.I. Leonidov, M.V. Ananyev, Oxygen isotope exchange in doped lanthanum zirconates, J. Solid State Chem. 268 (2018) 45–54.
[58] N.M. Porotnikova, V.A. Eremin, A.S. Farlenkov, E.K. Kurumchin, E.A. Sherstobitova, D.I. Kochubey, M.V. Ananyev, Effect of AO segregation on catalytical activity of $La_{0.7}A_{0.3}MnO_{3\pm\delta}$ (A = Ca, Sr, Ba) regarding oxygen reduction reaction, Catal. Lett. 148 (9) (2018) 2839–2847.
[59] M.M. Kuklja, E.A. Kotomin, R. Merkle, Y.A. Mastrikov, J. Maier, Combined theoretical and experimental analysis of processes determining cathode performance in solid oxide fuel cells, Phys. Chem. Chem. Phys. 15 (15) (2013) 5443–5471.
[60] T. Akbay, A. Staykov, J. Druce, H. Téllez, T. Ishihara, J.A. Kilner, The interaction of molecular oxygen on Lao terminated surfaces of La_2NiO_4, J. Mater. Chem. 4 (34) (2016) 13113–13124.
[61] A. Chroneos, D. Parfitt, J.A. Kilner, R.W. Grimes, Anisotropic oxygen diffusion in tetragonal $La_2NiO_{4+\delta}$: molecular dynamics calculations, J. Mater. Chem. 20 (2) (2010) 266–270.
[62] J.-M. Bassat, M. Burriel, O. Wahyudi, R. Castaing, M. Ceretti, P. Veber, I. Weill, A. Villesuzanne, J.-C. Grenier, W. Paulus, J.A. Kilner, Anisotropic oxygen diffusion properties in $Pr_2NiO_{4+\delta}$ and $Nd_2NiO_{4+\delta}$ single crystals, J. Phys. Chem. C 117 (50) (2013) 26466–26472.